F-wave pairing of cold atoms in optical lattices

Wei-Cheng Lee,[1,*] Congjun Wu,[1,†] and S. Das Sarma[2,‡]
[1]*Department of Physics, University of California, San Diego, California 92093, USA*
[2]*Condensed Matter Theory Center, Department of Physics, University of Maryland, College Park, Maryland 20742, USA*
(Received 1 August 2010; published 10 November 2010)

The tremendous development of cold atom physics has opened up a whole new opportunity to study novel states of matter which are not easily accessible in solid-state systems. Here we propose to realize the f-wave pairing superfluidity of spinless fermions in $p_{x,y}$-orbital bands of two-dimensional honeycomb optical lattices. The nontrivial orbital band structure, rather than strong correlation effects, gives rise to the unconventional pairing with the nodal lines of the f-wave symmetry. With a confining harmonic trap, zero-energy Andreev bound states appear around the circular boundary with a sixfold symmetry. The experimental realization and detection of this novel pairing state are feasible.

DOI: 10.1103/PhysRevA.82.053611 PACS number(s): 03.75.Ss, 75.50.Cc, 03.75.Mn, 71.10.Fd

I. INTRODUCTION

The study of unconventional Cooper pairing states has been a major subject in condensed matter physics for decades. In addition to isotropic s-wave pairing, many unconventional pairing states have been identified [1]. For example, different types of p-wave pairing states were found in superfluid ^{3}He systems [2,3] including the anisotropic chiral A phase and the isotropic B phase. Evidence of p-wave paring was also found in the ruthenate compound Sr_2RuO_4 [4,5]. The d-wave pairing states are most convincingly proved in high-T_c cuprates with phase-sensitive measurements including the Josephson tunneling junction [6,7] and zero-energy Andreev bound states [8,9]. Many heavy fermion compounds exhibit evidence of unconventional Cooper pairing such as UPt_3, UBe_{13}, and $CeCoIn_5$ with nodal points or lines [10–13]. However, conclusive experimental evidence to determine pairing symmetries is still lacking. These unconventional pairing states are driven by strong correlation effects, which brings significant difficulties to theoretical analysis and prediction. It would be great to find novel unconventional pairing mechanisms that are easier to handle.

In contrast, cold atom physics has recently become an emerging frontier for condensed matter physics [14–17]. In particular, the s-wave pairing superfluidity of fermions through Feshbach resonances has become a major research focus. Bose-Einstein condensation and Bardeen-Cooper-Schrieffer crossover have been extensively investigated [18–22]. Naturally, searching for unconventional Cooper pairing states in cold atom systems is expected to stimulate more exciting physics. For example, p-wave pairing states have been proposed using p-wave Feshbach resonances [23–25], which, however, suffer from the drawback of heavy particle loss. Unconventional Cooper pairing states with cold atoms have not been realized yet [26–29].

In this article, we propose an f-wave pairing state of spinless fermions in cold atom optical lattices. This unconventional pairing arises from the nontrivial band structure of $p_{x,y}$-orbital bands in honeycomb optical lattices combined with a conventional attractive interaction. The internal orbital configurations of Bloch-wave-band eigenstates vary with the crystal momenta, resulting in an f-wave angular form factor for the pairing order parameters. Along three high-symmetry lines in the Brillouin zone whose directions differ by 120° from each other, the intraband pairing order parameters are exactly suppressed to 0. The unconventional nature of this pairing is exhibited in the appearance of zero-energy Andreev bound states at the circular boundary upon imposition of a confining trap. Since no strong correlation effects are involved, our analysis here is well controllable. This is a novel state of matter, which, to our knowledge, has not been unambiguously identified before either in condensed matter or in cold atom systems, thus this result will greatly enrich the study of unconventional pairing states.

This article is organized as follows. In Sec. II, we explain the orbital structure of the Bloch-wave eigenstate in detail. In Sec. III, we show that f-wave Cooper pairing naturally arises from a conventional on-site Hubbard attraction. In Sec. IV, we discuss the zero-energy Andreev bound state at the edge of the confining trap, which provides phase-sensitive evidence. In Sec. V, we discuss experimental realization and detection. Conclusions are given in Sec. VI.

II. THE ORBITAL STRUCTURE OF THE *p*-BAND BLOCH-WAVE FUNCTIONS

The honeycomb optical lattice was experimentally constructed some years ago using three coplanar blue detuned laser beams whose wave vectors $\vec{k}_i$ $(i = 1,2,3)$ differ from each other by 120° [30]. After the lowest s-orbital band is fulfilled, the next active ones are $p_{x,y}$-orbital bands lying in the hexagonal plane. Differently from the situation in graphene, whose $p_{x,y}$-orbital bands hybridize strongly with the s-orbital bands and are pushed away from the Fermi surface, the hybridization between $p_{x,y}$ and s orbitals in the optical honeycomb lattice is negligible. The p_z-orbital band can be pushed to higher energies and thus unoccupied by imposition of strong confinement along the z axis. The $p_{x,y}$-orbital bands exhibit the characteristic features of orbital physics, that is, spatial anisotropy and orbital degeneracy. This provides an alternative

*leewc@physics.ucsd.edu
†wucj@physics.ucsd.edu
‡dassarma@umd.edu

perspective of the honeycomb lattice and is complementary to research focusing on the p_z-band system of graphene, which is not orbitally active. The alternative physics, which does not appear in graphene, includes the flat band structure [31], consequential nonperturbative strong correlation effects (e.g., Wigner crystal [32] and ferromagnetism [33]), frustrations in orbital exchange [34], and the quantum anomalous Hall effect [35].

We employ the $p_{x,y}$-orbital b and Hamiltonian studied in Refs. [31,32,34], and [35],

$$H_0 = t_\parallel \sum_{\vec{r}\in A, i=1,2,3} \{p^\dagger_{\vec{r},i} p_{\vec{r}+a\vec{e}_i,i} + \text{H.c.}\} - \mu \sum_{\vec{r}\in A\oplus B} n_{\vec{r}}, \quad (1)$$

where $\hat{e}_{1,2,3}$ are unit vectors from one site in sublattice A to its three neighboring sites in sublattice B, defined as $\hat{e}_{1,2} = \pm\frac{\sqrt{3}}{2}\hat{e}_x + \frac{1}{2}\hat{e}_y$, $\hat{e}_3 = -\hat{e}_y$; $p_i \equiv (p_x\hat{e}_x + p_y\hat{e}_y)\cdot\vec{e}_i$ is the p orbital projected onto the bond along the direction of $\hat{e}_i$, and only two of them are linearly independent; $n_{\vec{r}} = n_{\vec{r},x} + n_{\vec{r},y}$ is the particle number at site $\vec{r}$; the σ bonding $t_\parallel$ describes the hopping between p orbitals on neighboring sites parallel to the bond direction and is rescaled to 1 in the following; and a is the nearest-neighbor distance. $t_\parallel$ is positive due to the odd parity of p orbitals. Equation (1) neglects the π bonding $t_\perp$ describing the hopping between p orbitals perpendicular to the bond direction. Due to the high spatial anisotropy of the p orbitals, $t_\perp/t_\parallel \ll 1$. To confirm this, we have fitted $t_\perp$ and $t_\parallel$ from a realistic band structure calculation for the sinusoidal optical potential:

$$V(\vec{r}) = V_0 \sum_{1\leqslant i<j\leqslant 3} \cos\{(\vec{k}_i - \vec{k}_j)\cdot\vec{r}\}. \quad (2)$$

With a moderate potential depth of $V_0/E_R = 12$, $t_\perp/t_\parallel$ is already driven to 1% with $t_\parallel \approx 0.375E_R$, where $E_R = \frac{\hbar^2k^2}{2M}$ is the recoil energy and M is the atom mass. Further increasing V_0/E_R decreases $t_\perp/t_\parallel$ even more.

Equation (1) has a chiral symmetry, that is, under the transformation of $p_{\vec{r},x(y)} \to -p_{\vec{r},x(y)}$ only for sites in sublattice A, and not for sites in sublattice B, $H_0 \to -H_0$. Thus its four bands have symmetric spectra with respect to zero energy:

$$E_{1,4} = \mp\frac{3}{2}t_\parallel, \quad E_{2,3} = \mp\frac{t_\parallel}{2}\sqrt{3 + 2\sum_{i<j}\cos\vec{k}\cdot(\hat{e}_i - \hat{e}_j)}. \quad (3)$$

The Brillouin zone (BZ) is a regular hexagon with the edge length $\frac{4\pi}{3\sqrt{3}a}$. Two middle dispersive bands, 2 and 3, have two nonequivalent Dirac points $K(K') = (\pm\frac{4\pi}{3\sqrt{3}a}, 0)$, with a band width of $\frac{3}{2}t_\parallel$. The bottom and top bands are flat. We define the four-component annihilation operators in momentum space as $\hat{\phi}(\vec{k}) = [\hat{p}_{A,x}(\vec{k}), \hat{p}_{A,y}(\vec{k}), \hat{p}_{B,x}(\vec{k}), \hat{p}_{B,y}(\vec{k})]^T$. In this basis, the eigenoperator $\hat{\psi}_m(\vec{k})$ for band m can be diagonalized as $\hat{\psi}_m(\vec{k}) = \hat{\phi}_n(\vec{k})U_{nm}(\vec{k})$, where $U(\vec{k})$ is a 4×4 unitary matrix. The phase convention for band eigenvectors, that is, each column of $U(\vec{k})$, is conveniently chosen as $R_{\frac{\pi}{3}}\hat{\psi}_m(\vec{k})R_{\frac{\pi}{3}}^{-1} = \text{sgn}(m)\hat{\psi}_m(\vec{k}')$, with $\text{sgn}(m) = -$ for $m = 1,2$ and $\text{sgn}(m) = +$ for $m = 3,4$, where the symmetry operation $R_{\frac{\pi}{3}}$ is the 60° rotation around a center of the hexagonal plaquette and $\vec{k}' = R_{\frac{\pi}{3}}\vec{k}$. The analytical form of $U_{nm}(\vec{k})$ is given in Appendix A.

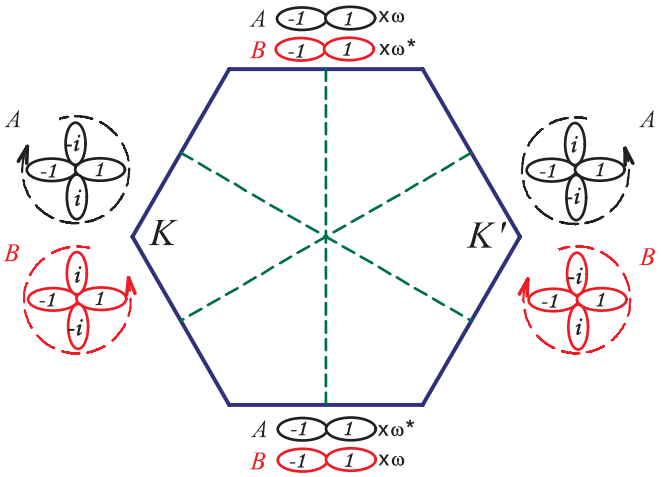

FIG. 1. (Color online) Orbital configurations of the lower dispersive band 2 at high-symmetry points and lines in the BZ. The time-reversal partners $\psi_2(\pm\vec{k})$ involve the same polar orbital only if $\vec{k}$ is along the three middle lines and take the complex orthogonal orbitals of $p_x \pm ip_y$ with opposite chiralities at $\vec{K}$ and $\vec{K}'$. $\omega = e^{i\frac{\pi}{6}}$.

The orbital configurations of the band eigenvectors have interesting patterns as depicted in Fig. 1, which arise from the lattice D_{6h} symmetry. Only the lowest dispersive band ($m = 2$) is plotted as an example. The lowest flat band ($m = 1$) has the same symmetry structure except for having different orbital polarization directions. The remaining two can be obtained by performing the operation of chiral symmetry. Six lines in the BZ possess reflection symmetry, that is, three passing the middle points of the opposite edges and three passing the opposite vertices of $\vec{K}$ and $\vec{K}'$. The eigenvectors of each band along these lines should be either even or odd with respect to the corresponding reflection. For example, for reflection with respect to the y axis, the orbitals transform as

$$\hat{p}_{A(B),x} \to -\hat{p}_{A(B),x}, \quad \hat{p}_{A(B),y} \to \hat{p}_{A(B),y}, \quad (4)$$

thus the eigenoperators $\hat{\psi}_m(\vec{k})$ with $\vec{k} \parallel \hat{y}$ must be either purely $\hat{p}_y$ (even) or $\hat{p}_x$ (odd). For the other two middle lines, the corresponding eigenvectors are obtained by performing the $\pm 120^\circ$ rotation. For the time-reversal partners $\hat{\psi}_m(\vec{k})$ and $\hat{\psi}_m(-\vec{k})$ along these lines, they only take the same real polar orbitals. In contrast, the reflection with respect to the x axis gives rise to the transformation

$$\hat{p}_{A(B),x} \to \hat{p}_{B(A),x}, \quad \hat{p}_{A(B),y} \to -\hat{p}_{B(A),y}. \quad (5)$$

Furthermore, $\vec{K}$ and $\vec{K}'$ have threefold rotational symmetry. Combining two facts, $\hat{\psi}_m(\vec{K})$ should be $p_x + ip_y$ for sites in one of the sublattices and $p_x - ip_y$ for sites in the other sublattice. Its time-reversal partner $\hat{\psi}_m(\vec{K}')$ has the opposite chiralities in both sublattices with respect to those at $\vec{K}$. In other words, the orbital configurations of $\hat{\psi}_m(\vec{k})$ are linearly polarized at the middle points of the BZ edge, change to being circularly polarized at the vertices, and are elliptically polarized in between.

III. F-WAVE COOPER PAIRING

Next we introduce the on-site attractive interaction term between spinless fermions,

$$H_{\rm int} = -U \sum_{\vec{r}} n_{\vec{r},x} n_{\vec{r},y}, \tag{6}$$

where U is positive. We perform the mean-field decomposition for $H_{\rm int}$ in the pairing channel,

$$H_{\rm int}^{\rm pairing} = -\sum_{\vec{r}_{A,B}} \{\Delta_A^* p_{\vec{r}_A,y} p_{\vec{r}_A,x} + \Delta_B^* p_{\vec{r}_B,y} p_{\vec{r}_B,x} + {\rm H.c.}\}$$
$$= \sum_{\vec{k}}{}' \sum_{m,n=1}^{4} \Delta_{nm}^*(\vec{k}) \psi_n(\vec{k}) \psi_m(-\vec{k}) + {\rm H.c.}, \tag{7}$$

where the pairing order parameters in the A and B sublattices are self-consistently defined as $\Delta_{A(B)}^* = U\langle G| p_{r_{A(B),x}}^\dagger p_{r_{A(B),y}}^\dagger |G\rangle$; $\langle G|\cdots|G\rangle$ is the average over the pairing ground state; the summation of $\vec{k}$ covers only half of the BZ; and the multiband pairing order parameters in momentum space have a 4×4 matrix structure,

$$\Delta_{nm}(\vec{k}) = U\langle G|\psi_n(\vec{k})\psi_m(-\vec{k})|G\rangle. \tag{8}$$

Under the rotation of $R_{\frac{\pi}{3}}$, it transforms as $R_{\frac{\pi}{3}} \Delta_{nm}(\vec{k}) R_{\frac{\pi}{3}}^{-1} = {\rm sgn}(n)\,{\rm sgn}(m)\Delta_{nm}(\vec{k}')$.

In addition, we also introduce the mean-field decomposition for $H_{\rm int}$ in the charge-density wave (CDW) channel:

$$H_{\rm int}^{\rm CDW} = \sum_{\vec{r}_{A,B},\tau=x,y} \left(-Un - \frac{N}{2}\right) p_{\vec{r}_A,\tau}^\dagger p_{\vec{r}_A,\tau}$$
$$+ \left(-Un + \frac{N}{2}\right) p_{\vec{r}_B,\tau}^\dagger p_{\vec{r}_B,\tau}, \tag{9}$$

where

$$n = \langle G|\left(n_{\vec{r}_A,x} + n_{\vec{r}_A,y} + n_{\vec{r}_B,x} + n_{\vec{r}_B,y}\right)/2|G\rangle \tag{10}$$

is the total particle filling, and

$$N = U\langle G|\left(n_{\vec{r}_A,x} + n_{\vec{r}_A,y} - n_{\vec{r}_B,x} - n_{\vec{r}_B,y}\right)|G\rangle \tag{11}$$

is the CDW order parameter. Generally speaking, the CDW becomes important in large U or close to half-filling ($n = 1$), as discussed here.

The intraband gap functions Δ_{nn} can be calculated analytically as $\Delta_{nn}(\vec{k}) = i(-)^n \frac{1}{2}(\Delta_A - \Delta_B)F(\vec{k})$, with the f-wave form factor of

$$F(\vec{k}) = \frac{16}{\sqrt{3}N_0(\vec{k})} \sin\frac{\sqrt{3}}{2}k_x \left[\cos\frac{\sqrt{3}}{2}k_x - \cos\frac{3}{2}k_y\right], \tag{12}$$

where N_0 satisfies

$$N_0(\vec{k}) = \frac{8}{3}\left\{3 - \sum_{1\leqslant i<j\leqslant 3} \cos\vec{k}\cdot(\hat{e}_i - \hat{e}_j)\right\}. \tag{13}$$

Δ_A can be fixed positive, and $\Delta_B = |\Delta_B| e^{i\Delta\theta}$ with a relative phase $\Delta\theta$. The optimal $\Delta\theta$ takes the value of π, that is, $\Delta_A = -\Delta_B$, to maximize the intraband pairings. We have confirmed this in the explicit self-consistent mean-field solution for Eqs. (1) and (7). Furthermore, the nonvanishing π-bonding $t_\perp$ term can further stabilize this solution as a result of the odd parity of π orbitals.

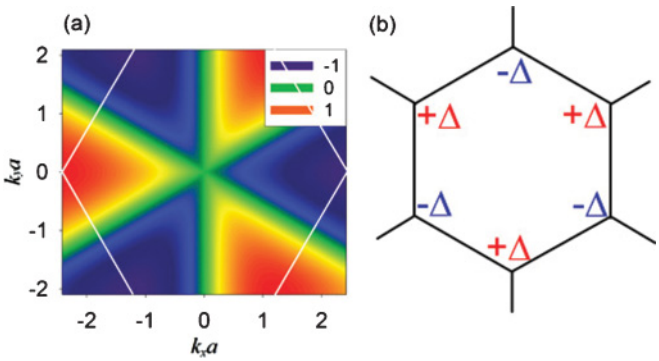

FIG. 2. (Color online) (a) The f-wave pairing form factor $F(\vec{k})$ for intraband pairing in momentum space. (b) The f-wave pairing pattern in real space with $\Delta_A = -\Delta_B = \Delta$.

Now we discuss the pairing symmetry of this system. Since the fermions are spinless, the pairing wave function is expected to have odd parity due to the antisymmetry requirement of the fermionic many-body wave functions, and p-wave symmetry with the lowest angular momentum seems to be the leading candidate. Nevertheless, we find that the configuration of $\Delta_A = -\Delta_B = \Delta$ exhibits f-wave symmetry; that is, the rotation of $R_{\frac{\pi}{3}}$ is equivalent to flipping the sign of Δ as depicted in Fig. 2(a). In particular, the diagonal terms satisfy

$$R_{\frac{\pi}{3}} \Delta_{nn}(\vec{k}) R_{\frac{\pi}{3}}^{-1} = -\Delta_{nn}(\vec{k}) \tag{14}$$

as exhibited in $F(\vec{k})$ with three nodal lines of $k_x = 0, k_y = \pm k_x/\sqrt{3}$. These are the same middle lines marked in Fig. 1 along which the time-reversal partners $\psi_n(\pm\vec{k})$ have the same polar orbital configurations. The pairing amplitude vanishes along these lines because interaction exists only between two orthogonal orbitals. In contrast, maximal pairings occur between $\vec{K}$ and $\vec{K}'$ with opposite signs whose orbital configurations are orthogonal to each other. In order words, the property of the reflection symmetry of the $p_{x,y}$ orbitals leads to vanishing of the intraband pairing interaction along three nodal lines. As a result, the pairing state favors f-wave over p-wave symmetries in order to match the nodal lines of the pairing interactions. It is emphasized that, unlike other examples of unconventional pairing in condensed matter systems, this f-wave pairing structure mainly arises from the nontrivial orbital configuration of band structures but with conventional interactions.

We next study the pairing strength $\Delta_A = -\Delta_B = \Delta$ in the weak coupling regime with $U/t_\parallel = 2.2$, in which the validity of the self-consistent mean-field theory is justified. The lattice chiral symmetry ensures that these results are symmetric with respect to the filling $n = 1$, so that we present the results only for $n \leqslant 1$. The case of $0 < n < 0.5$ corresponds to filling in the bottom flat band in which each band eigenstate can be constructed to be localized within the single hexagon plaquette present (see Refs. [31] and [34]). The attractive interaction drives all the plaquette states to touch each other, leading to phase separation until the flat band is filled, which will be discussed in a future publication. In Fig. 3(a), we plot Δ for

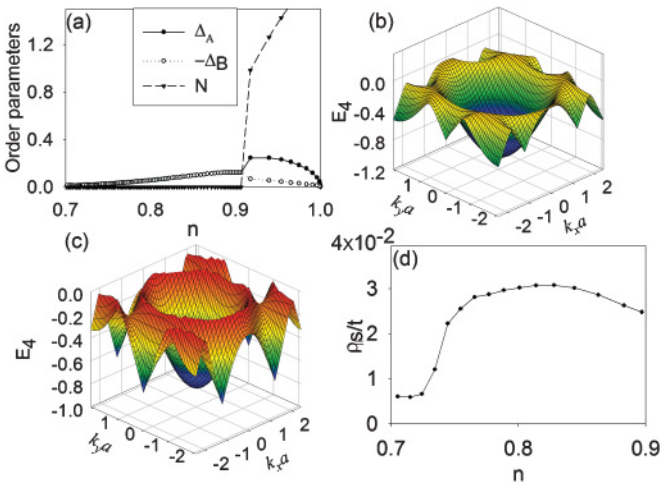

FIG. 3. (Color online) Gap and superfluid density for the f-wave state at $U/t_\parallel = 2.2$ and $0.7 < n < 1.0$. (a) The pairing amplitude $\Delta_A = -\Delta_B = \Delta$ until $n \approx 0.9$. For $n > 0.9$, the CDW order starts to coexist with the f-wave pairing superfluid, resulting in an f-wave supersolid state. (b, c) Lowest-energy branch of Bogoliubov excitations at $n = 0.89$ and $n = 0.78$. For a better visual effect, only negative eigenvalues are shown. (d) Superfluid density ρ_s vs. n.

$0.7 < n < 1.0$, which corresponds to filling in the dispersive bands. It is shown that the pairing state remains purely f wave until $n \approx 0.9$. For $n > 0.9$, the CDW order parameter N becomes nonzero due to the strong nesting near half-filling, and it contributes an s-wave component to the interband pairing, resulting in $\Delta_A \neq -\Delta_B$, shown in Fig. 3(a). Since the CDW order coexists with the pairing superfluid with a dominant f-wave component, the phase in the region of $0.9 < n < 1.0$ is the f-wave supersolid state, which is also an alternate phase not seen in other systems.

Due to the multiband structure, this f-wave pairing state remains fully gapped for general values of $U/t_\parallel$ and n. We plot the branch of the lowest-energy Bogoliubov excitations for $U/t_\parallel = 2.2$ and the filling $0.7 < n < 1$, where the Fermi energy lies in band 2. For n close to 1 in Fig. 3(b) ($n = 0.89$), the Fermi surfaces form two disconnected pockets around the $\vec{K}$ and $\vec{K}'$ away from the nodal lines of $\Delta_{22}(\vec{k})$, thus the spectra are gapped. As n is lowered in Fig. 3(c) ($n = 0.78$), the Fermi surface becomes connected and intersects with the nodal lines of Δ_{22}. At these intersections, the system in general remains gapped because of the nonzero interband pairing $\Delta_{12}(\vec{k})$.

The superfluid density ρ_s is plotted in Fig. 3(d) for $0.7 < n < 1.0$ and $U/t_\parallel = 2.2$, which is defined as

$$\rho_s \equiv \frac{\hbar^2}{2m^*} n_s = \lim_{\delta\theta \to 0} \frac{1}{2} \frac{\partial^2 E_{\mathrm{MF}}}{\partial \delta\theta^2}, \tag{15}$$

where $\delta\theta$ is the phase twist across the system boundaries. The behavior of ρ_s is very different from that of the pairing gap, which is mostly determined by the states in the dispersive band. ρ_s reaches the maximal value of about $0.03t_\parallel$ around $n = 0.82$ because the filling is close to the van Hove singularity of the density of states and then drops as we approach the Dirac points at $n = 1$. In two-dimensional systems, the superfluidity develops below the Kosterlitz-Thouless (KT) transition temperature $T_{\mathrm{KT}} \approx \frac{\pi}{2}\rho_s$.

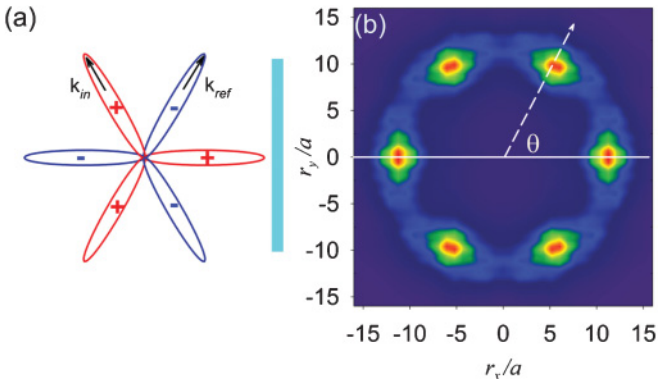

FIG. 4. (Color online) (a) Zero-energy Andreev bound states appear on the boundary perpendicular to the antinodal directions. (b) The zero-energy L_{DOS} in real space with the maximal value at $\theta = n\pi/3$ is a signature of the f-wave pairing symmetry.

The preceding mechanism for f-wave pairing works in weak coupling systems where the nontrivial orbital band structure in momentum space is essential. In contrast, in the strong coupling limit, that is, where U is much larger than the band width, Cooper pairing occurs in real space. Two fermions in the same site form a Cooper pair which can tunnel to neighboring sites. As explained in Ref. [41], due to the odd parity of the p orbitals, the Josephson coupling amplitude is positive, which favors a phase difference of π between two neighbors. Furthermore, its amplitude is much lower than that of the CDW coupling because the π bonding $t_\perp$ is much smaller than $t_\parallel$. As a result, the superfluid density is very low in the strong coupling limit, although the pairing gap is of the order of U.

IV. ZERO-ENERGY ANDREEV BOUND STATES

One of the most convincing proofs of the unconventional pairing is the existence of the zero-energy Andreev bound states at boundaries because of their phase sensitivity [8]. Figure 4(a) depicts the situation of the boundary perpendicular to the antinodal lines of the intraband pairing. The scattering of the Bogoliubov quasiparticles changes momentum from $\vec{k}_{\mathrm{in}}$ to $\vec{k}_{\mathrm{ref}}$, along which the pairing parameters switch sign as $\Delta_{nn}(\vec{k}_{\mathrm{in}}) = -\Delta_{nn}(\vec{k}_{\mathrm{ref}})$, which gives rise to zero-energy Andreev bound states. In contrast, if the boundary is perpendicular to the nodal lines, no phase changes occur and thus Andreev bound states vanish.

Naturally in experimental systems with an overall confining trap, the circular edge boundary samples all the orientations. We performed a real-space Bogoliubov–de Gennes calculation [36],

$$\begin{pmatrix} \hat{H} & \hat{\Delta} \\ \hat{\Delta}^* & -\hat{H} \end{pmatrix} \begin{pmatrix} u_n(i) \\ v_n(i) \end{pmatrix} = E_n \begin{pmatrix} u_n(i) \\ v_n(i) \end{pmatrix}, \tag{16}$$

where i is the site index in real space, $H = H_0 + V_{\mathrm{ex}}$, $V_{\mathrm{ex}} = \frac{m}{2}\Omega^2 r_i^2$ is the harmonic confining potential with parameters $m\Omega^2 a^2 = 0.001t_\parallel$, and r_i is the distance from the center of the confining potential to site i. To simulate the realistic

experimental situation better, we also add the π-bonding term [32], hopping in the direction *perpendicular* to the bond direction, into H_0, and the hopping integral is estimated to be $t_\perp/t_\parallel = -0.1$. The local density of states ($L_{\rm DOS}$) at energy E is defined as

$$LD(\vec{r},E) = \frac{1}{N}\sum_n |u_n(\vec{r})|^2\delta(E-E_n) + |v_n(\vec{r})|^2\delta(E+E_n), \quad (17)$$

where N is the total number of lattice sites. The numerical result of the zero-energy $LD(\vec{r},0)$ is depicted in real space in Fig. 4(b), with the parameter values $U/t_\parallel = 2.5$ and $\mu = -1.58$, which correspond to the filling in the center of the trap $n_c = 0.88$. Figure 4(b) shows that $LD(\vec{r},0)$ is nonzero only at sites near the boundary, signaling the existence of zero-energy Andreev bound states with sixfold symmetry. The $L_{\rm DOS}$ maxima occur at angles $\theta = n\frac{\pi}{3}$ ($n = 1$–6), which are perpendicular to the antinodal directions shown in Fig. 4(a), and the minima are located at $\theta = (n+\frac{1}{2})\frac{\pi}{3}$. As U increases, the CDW order starts to coexist with the f-wave pairing, and it introduces s-wave interband pairings into the system. Consequently, the scattering process of Bogoliubov quasiparticles described in Fig. 4(a) no longer has a complete sign change in the pairing parameters as discussed previously. In this case, we still find Andreev bound states with sixfold symmetry up to $U/t_\parallel = 3$, except that they have finite energy below the excitation gap instead of zero energy.

The zero-energy Andreev bound states of this f-wave state are different from those of the $p_x + ip_y$ pairing state. The f-wave pairing symmetry presented here is real and anisotropic, which maintains time-reversal symmetry. The edge responses are also anisotropic: the spectra of the zero-energy Andreev state are strongest along the boundaries perpendicular to the antinodal direction. In contrast, the $p_x + ip_y$ pairing symmetry is complex. The spatial rotation operation on the $p_x + ip_y$ state is equivalent to the change of the global pairing phase, thus its responses to all the boundaries with different directions are the same. Edge states appear regardless of the directions of the boundaries. Furthermore, due to its breaking time-reversal symmetry, the edge states in the $p_x + ip_y$ states carry currents.

V. EXPERIMENTAL REALIZATION AND DETECTION

The experimental realization of this novel f-wave state is feasible. To enhance the attractive interaction between spinless fermions, we propose to use atoms with large magnetic moments, such as ^{167}Er with $m = 7\mu_B$, on which laser cooling has been performed [37]. Compared to another possibility, using the p-wave Feshbach resonance, this method has the advantage of maintaining the system's stability. The interaction between two fermions in $p_{x,y}$ orbitals reads

$$-U = \int d^3\vec{r}_1 d^3\vec{r}_2 V(\vec{r}_1-\vec{r}_2)\{[\psi_{p_x}(\vec{r}_1)\psi_{p_y}(\vec{r}_2)]^2 - \psi^*_{p_x}(\vec{r}_1)\psi^*_{p_y}(\vec{r}_2)\psi_{p_x}(\vec{r}_2)\psi_{p_y}(\vec{r}_1)\}, \quad (18)$$

where ψ_{p_x,p_y} are Wannier wave functions. The overall dipole interaction can be made attractive by polarizing the magnetic moments parallel to the hexagonal plane, which gives rise to $V(\vec{r}_1-\vec{r}_2) = m^2(1-3\cos^2\theta)/r^3$, where $r = |\vec{r}_1-\vec{r}_2|$ and θ is the angle between $\vec{m}$ and $\vec{r}_1-\vec{r}_2$. We take the laser wavelength $\lambda \approx 600$ nm and then the recoil energy $E_R = 157$ nK. As shown in the Supplementary Information, by choosing $V_0/E_R = 30$, the estimation shows that $U \approx 96$ nK and $t_\parallel \approx 0.2E_R = 31$ nK, and thus $U/t_\parallel \approx 3$ as already chosen. As shown in Fig. 3(d), the maximal $T_{\rm KT} \approx \frac{\pi}{2}(0.02t_\parallel) \approx 1 \sim 2$ nK, which is within the experimentally accessible regime.

Successful detection of zero-energy Andreev bound states will be convincing proof of the f-wave pairing state. Radiofrequency (rf) spectroscopy has been an established tool for determining the pairing gap in cold atom systems [19,38]. It also has a good spatial resolution [39], which makes direct imaging of the spatial distribution of zero-energy Andreev bound states feasible. The unique symmetry pattern of zero-energy Andreev bound states localized at the trap boundary can be revealed by identifying the locations of the zero-energy spectrum determined from spatially resolved rf spectroscopy. Even for the case in which the Andreev bound states are not at zero energy due to the CDW order, since they are the lowest-energy states and below the excitation gap, one can still find that the lowest-energy spectra appear near the six locations shown in Fig. 4(b).

VI. DISCUSSION AND CONCLUSION

In summary, we have proposed the realization of a novel f-wave pairing state with spinless fermions which has not been identified in solid-state and cold atom systems before. The key reason is the nontrivial p-orbital band structure of the honeycomb lattice rather than the strong correlation physics, which renders the preceding analysis controllable. The $T_{\rm KT}$ is estimated to reach the order of 1 nK within experimental accessibility. rf spectroscopy detection of the sixfold symmetry pattern of zero-energy Andreev bound states along the circular boundary will provide a phase-sensitive test of f-wave symmetry.

ACKNOWLEDGMENTS

C.W. acknowledges the Aspen Center for Physics, where this work was initiated. C.W. and W.C.L. were supported by Grants No. NSF-DMR 0804775 and ARO-W911NF0810291. S.D.S. was supported by the ARO-DARPA and NSF-PFC.

APPENDIX A: EIGENVECTORS OF THE BAND HAMILTONIAN AND THE PAIRING MATRIX

In this section, we present the spectra of the band Hamiltonian, Eq. (1), and the pairing matrix Δ_{mn}. With the four-component spinor operator defined as

$$\hat{\phi}(\vec{k}) = \left[p_{Ax}(\vec{k}), p_{Ay}(\vec{k}), p_{Bx}(\vec{k}), p_{By}(\vec{k})\right]^T, \quad (A1)$$

Eq. (1) becomes

$$H_0 = t_\parallel \sum_k \hat{\phi}^\dagger_m(\vec{k}) H_{0,mn}(\vec{k}) \hat{\phi}_n(\vec{k}), \quad (A2)$$

where the matrix kernel $H_{0,mn}(\vec{k})$ takes the structure

$$\begin{pmatrix} 0 & 0 & \frac{3}{4}(e^{i\vec{k}\cdot\vec{e}_1}+e^{i\vec{k}\cdot\vec{e}_2}) & \frac{\sqrt{3}}{4}(e^{i\vec{k}\cdot\vec{e}_1}-e^{i\vec{k}\cdot\vec{e}_2}) \\ 0 & 0 & \frac{\sqrt{3}}{4}(e^{i\vec{k}\cdot\vec{e}_1}-e^{i\vec{k}\cdot\vec{e}_2}) & \frac{1}{4}(e^{i\vec{k}\cdot\vec{e}_1}+e^{i\vec{k}\cdot\vec{e}_2})+e^{i\vec{k}\cdot\vec{e}_3} \\ \text{H.c.} & & 0 & 0 \\ & & 0 & 0 \end{pmatrix}.$$

For each momentum $\vec{k}$, $H_0(\vec{k})$ is diagonalized as

$$H_{0,lm}(\vec{k})U_{mn} = E_l U_{ln}. \tag{A3}$$

The band eigenoperators are expressed as

$$\hat{\psi}_m(\vec{k}) = \hat{\phi}_n(\vec{k})U_{nm}(\vec{k}). \tag{A4}$$

The unitary matrix $U(\vec{k})$ reads

$$U(\vec{k}) = \begin{pmatrix} a^*(\vec{k}) & e^{-i\frac{\theta_k}{2}}b(\vec{k}) & e^{-i\frac{\theta_k}{2}}b(\vec{k}) & a^*(\vec{k}) \\ -b^*(\vec{k}) & e^{-i\frac{\theta_k}{2}}a(\vec{k}) & e^{-i\frac{\theta_k}{2}}a(\vec{k}) & -b^*(\vec{k}) \\ a(\vec{k}) & e^{i\frac{\theta_k}{2}}b^*(\vec{k}) & -e^{i\frac{\theta_k}{2}}b^*(\vec{k}) & -a(\vec{k}) \\ -b(\vec{k}) & e^{i\frac{\theta_k}{2}}a^*(\vec{k}) & -e^{i\frac{\theta_k}{2}}a^*(\vec{k}) & b(\vec{k}) \end{pmatrix}, \tag{A5}$$

where

$$\begin{aligned} a(\vec{k}) &= \frac{f_{23}(\vec{k})-f_{31}(\vec{k})}{\sqrt{3N_0(\vec{k})}}; \quad b(\vec{k}) = \frac{f_{12}(\vec{k})}{\sqrt{N_0(\vec{k})}}; \\ \theta_k &= \arg\left(\sum_i e^{i\vec{k}\cdot\hat{e}_i}\right) \in [-\pi,\pi); \\ f_{ij}(\vec{k}) &= e^{i\vec{k}\cdot\hat{e}_i} - e^{i\vec{k}\cdot\hat{e}_j}; \\ N_0(\vec{k}) &= \frac{8}{3}\left[3 - \sum_{1\leqslant i<j\leqslant 3}\cos\vec{k}\cdot(\hat{e}_i-\hat{e}_j)\right]. \end{aligned} \tag{A6}$$

Using the eigenvector matrix $U(\vec{k})$, the pairing matrix Δ_{mn} can be spelled out straightforwardly as

$$\begin{aligned} \Delta_{mn}(\vec{k}) = {} & \Delta_A[\hat{U}_{2m}(-\vec{k})\hat{U}_{1n}(\vec{k}) - \hat{U}_{1m}(-\vec{k})\hat{U}_{2n}(\vec{k})] \\ & + \Delta_B[\hat{U}_{4m}(-\vec{k})\hat{U}_{3n}(\vec{k}) - \hat{U}_{3m}(-\vec{k})\hat{U}_{4n}(\vec{k})]. \end{aligned} \tag{A7}$$

For the solution of $\Delta_A = -\Delta_B = \Delta$, we have the pairing matrix

$$\Delta(\vec{k}) = \begin{pmatrix} \Delta_1(\vec{k}) & \Delta_2(\vec{k}) & \Delta_3(\vec{k}) & 0 \\ \Delta_2(\vec{k}) & -\Delta_1(\vec{k}) & 0 & -\Delta_3(\vec{k}) \\ -\Delta_3(\vec{k}) & 0 & -\Delta_1(\vec{k}) & \Delta_2(\vec{k}) \\ 0 & \Delta_3(\vec{k}) & \Delta_2(\vec{k}) & \Delta_1(\vec{k}) \end{pmatrix}, \tag{A8}$$

where the matrix elements read

$$\begin{aligned} \Delta_1(\vec{k}) &= i\frac{16\Delta}{\sqrt{3}N_0(\vec{k})}\sin\frac{\sqrt{3}}{2}k_x\left[\cos\frac{\sqrt{3}}{2}k_x - \cos\frac{3}{2}k_y\right], \\ \Delta_2(\vec{k}) &= i\frac{16\Delta}{3N_0(\vec{k})}\left[K_1(\vec{k})\sin\frac{\theta_k}{2} + K_2(\vec{k})\cos\frac{\theta_k}{2}\right], \\ \Delta_3(\vec{k}) &= \frac{16\Delta}{3N_0(\vec{k})}\left[K_1(\vec{k})\cos\frac{\theta_k}{2} - K_2(\vec{k})\sin\frac{\theta_k}{2}\right], \end{aligned} \tag{A9}$$

and

$$\begin{aligned} K_1(\vec{k}) = {} & 4\cos^4\frac{k_y}{2} + \left(4\cos^2\frac{\sqrt{3}}{2}k_x - 7\right)\cos^2\frac{k_y}{2} \\ & - \cos\frac{k_y}{2}\cos\frac{\sqrt{3}}{2}k_x + 2\sin^2\frac{\sqrt{3}}{2}k_x, \\ K_2(\vec{k}) = {} & \sin\frac{k_y}{2}\left(\cos\frac{\sqrt{3}}{2}k_x - \cos\frac{k_y}{2}\right) \\ & \times\left[\left(2\cos\frac{k_y}{2} + \cos\frac{\sqrt{3}}{2}k_x\right)^2 + \sin^2\frac{\sqrt{3}}{2}k_x\right]. \end{aligned} \tag{A10}$$

Both the band Hamiltonian, Eq. (1), and the interaction, Eq. (6), are invariant under the rotation $R_{\frac{\pi}{3}}$. Applying $R_{\frac{\pi}{3}}$ to the band Hamiltonian matrix in momentum space $H_0(\vec{k})$, it transforms as

$$H_0\left[\vec{k}' = R_{\frac{\pi}{3}}(\vec{k})\right] = R_{\frac{\pi}{3}}H_0(\vec{k})R_{\frac{\pi}{3}}^{-1}, \tag{A11}$$

where $R_{\frac{\pi}{3}}$ is defined as

$$R_{\frac{\pi}{3}} = \begin{pmatrix} 0 & r_{\frac{\pi}{3}} \\ r_{\frac{\pi}{3}} & 0 \end{pmatrix}, \tag{A12}$$

and

$$r_{\frac{\pi}{3}} = \begin{pmatrix} \cos\frac{\pi}{3} & -\sin\frac{\pi}{3} \\ \sin\frac{\pi}{3} & \cos\frac{\pi}{3} \end{pmatrix}. \tag{A13}$$

Correspondingly, it can be shown directly that

$$R_{\frac{\pi}{3}}\hat{\psi}_m(\vec{k}) = \mathrm{sgn}(m)\hat{\psi}_m(\vec{k}'), \tag{A14}$$

with $\mathrm{sgn}(m) = -1$ for $m = 1,2$ and $+1$ for $m = 3,4$, and $R_{\frac{\pi}{3}}\Delta_{mn}(\vec{k})R_{\frac{\pi}{3}}^{-1} = \mathrm{sgn}(n)\mathrm{sgn}(m)\Delta_{mn}(\vec{k}')$.

APPENDIX B: CALCULATION OF THE ON-SITE HUBBARD INTERACTION WITH MAGNETIC DIPOLAR INTERACTION

The optical potential around the center of each optical site can be approximated as

$$V(\vec{r}) = \frac{m}{2}\omega^2\left(r_x^2 + r_y^2\right) + \frac{m}{2}\omega_z^2 r_z^2, \tag{B1}$$

where we assume that the confinement on the z axis is stronger, so that $\omega_z > \omega$. The wave functions for the p_x and p_y orbitals in this harmonic potential are

$$\begin{aligned} \psi_{p_x}(\vec{r}) &= C^{\frac{1}{2}}r_x\exp\left\{-\frac{r_x^2+r_y^2}{2l^2} - \frac{r_z^2}{2l_z^2}\right\}, \\ \psi_{p_y}(\vec{r}) &= C^{\frac{1}{2}}r_y\exp\left\{-\frac{r_x^2+r_y^2}{2l^2} - \frac{r_z^2}{2l_z^2}\right\}, \end{aligned} \tag{B2}$$

where $C = 2l^{-4}l_z^{-1}\pi^{-3/2}$, $l = \sqrt{\hbar/m\omega}$, $l_z = \sqrt{\hbar/m\omega_z}$, and $l_z < l$.

With these wave functions, the on-site interaction can be evaluated with the direct and exchange terms:

$$\begin{aligned} -U &= \int d^3\vec{r}_1 d^3\vec{r}_2 V(\vec{r}_1-\vec{r}_2)\{[\psi_{p_x}(\vec{r}_1)\psi_{p_y}(\vec{r}_2)]^2 \\ &\quad -\psi^*_{p_x}(\vec{r}_1)\psi^*_{p_y}(\vec{r}_2)\psi_{p_x}(\vec{r}_2)\psi_{p_y}(\vec{r}_1)\} \\ &= C^2\int d^3\vec{r}d^3\vec{R}V(\vec{r})\left(\frac{R_x^2r_y^2+R_y^2r_x^2}{2}\right) \\ &\quad \times F_1(\vec{r})F_2(\vec{R}), \end{aligned} \tag{B3}$$

where we have introduced the relative coordinate $\vec{r}=\vec{r}_1-\vec{r}_2$ and the center-of-mass coordinate $\vec{R}=(\vec{r}_1+\vec{r}_2)/2$, and defined

$$\begin{aligned} F_1(\vec{r}) &= \exp\left\{-\frac{r_x^2+r_y^2}{2l^2}-\frac{r_z^2}{2l_z^2}\right\}, \\ F_2(\vec{R}) &= \exp\left\{-\frac{2(R_x^2+R_y^2)}{l^2}-\frac{2R_z^2}{l_z^2}\right\}. \end{aligned} \tag{B4}$$

We propose to use fermionic atoms with large magnetic dipole moments $\vec{m}$. Upon polarization of the magnetic moments with an external magnetic field, the anisotropic interaction reads

$$V(\vec{r}) = \frac{\mu_0}{4\pi}\frac{m^2[1-3(\hat{m}\cdot\hat{r})]^2}{r^3}, \tag{B5}$$

where $\hat{m}=\vec{m}/m$ and $\hat{r}=\vec{r}/r$, respectively. We assume that the polarization angle between $\vec{m}$ and the xy plane is θ, and perform the Gaussian integrals in Eq. (B3). The result is expressed analytically as

$$-U = \frac{\mu_0}{4\pi}\frac{m^2}{2l^3}\left(1-\frac{3}{2}\cos^2\theta\right)F(y), \tag{B6}$$

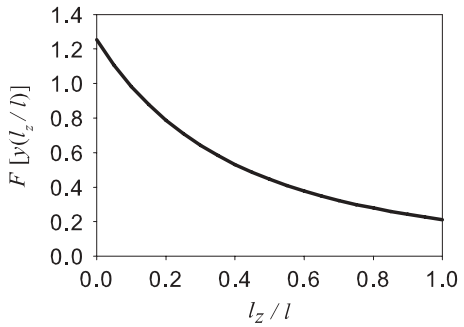

FIG. 5. $F[y(l_z/l)]$ as a function of l_z/l.

where

$$F(y) = \sqrt{\frac{2}{\pi}}(1+y)^{3/2}\left[(3y+1)\tan^{-1}\left(\frac{1}{\sqrt{y}}\right)-3\sqrt{y}\right], \tag{B7}$$

and y is a function of l_z/l as $y(l_z/l)=l_z^2/(l^2-l_z^2)$. $F[y(l_z/l)]$ is a monotonic decreasing function of l_z as shown in Fig. 5, which reflects that wave functions with a larger l_z have smaller overlaps with each other.

The largest attractive interaction can be achieved by polarizing the magnetic moments in the xy plane. If we use a fermionic atom of ^{167}Er with $m=7\mu_B$ and a laser beam with the wavelength $\lambda\approx 600$ nm to construct the honeycomb optical lattice, the recoil energy $E_R=h^2/2m\lambda^2=157$ nK and $l\approx 93(\frac{E_R}{V_0})^{1/4}$ nm. Compared to the realistic band structure calculation with $V_0/E_R=30$ in Ref. [34], $t_\parallel$ is fitted as $t_\parallel\approx 0.2E_R=31$ nK and $l\approx 40$ nm. With the choice of $l_z/l=0.2$, U reaches 96 nK, thus $U/t_\parallel\approx 3$, employed in this paper, is achieved. Recently, a large number of fermionic atoms ^{163}Dy with $m=10\mu_B$ has been successfully cooled and trapped [40]. For this atom, the recoil energy $E_R=h^2/2m\lambda^2=161$ nK, and $U/t_\parallel\approx 3$ can be achieved with the choice of $l_z/l=0.55$.

[1] M. Sigrist and K. Ueda, Rev. Mod. Phys. **63**, 239 (1991).
[2] A. J. Leggett, Rev. Mod. Phys. **47**, 331 (1975).
[3] D. D. Osheroff, Rev. Mod. Phys. **69**, 667 (1997).
[4] K. Nelson, Z. Mao, Y. Maeno, and Y. Liu, Science **306**, 1151 (2004).
[5] F. Kidwingira, J. Strand, D. J. V. Harlingen, and Y. Maeno, Science **314**, 1267 (2006).
[6] D. J. Van Harlingen, Rev. Mod. Phys. **67**, 515 (1995).
[7] C. C. Tsuei and J. R. Kirtley, Rev. Mod. Phys. **72**, 969 (2000).
[8] C.-R. Hu, Phys. Rev. Lett. **72**, 1526 (1994).
[9] G. Deutscher, Rev. Mod. Phys. **77**, 109 (2005).
[10] R. Joynt and L. Taillefer, Rev. Mod. Phys. **74**, 235 (2002).
[11] D. E. MacLaughlin, C. Tien, W. G. Clark, M. D. Lan, Z. Fisk, J. L. Smith, and H. R. Ott, Phys. Rev. Lett. **53**, 1833 (1984).
[12] K. Izawa, H. Yamaguchi, Y. Matsuda, H. Shishido, R. Settai, and Y. Onuki, Phys. Rev. Lett. **87**, 057002 (2001).
[13] J. D. Strand, D. J. Van Harlingen, J. B. Kycia, and W. P. Halperin, Phys. Rev. Lett. **103**, 197002 (2009).
[14] F. Dalfovo, S. Giorgini, L. P. Pitaevskii, and S. Tringari, Rev. Mod. Phys. **71**, 463 (1999).
[15] A. J. Leggett, Rev. Mod. Phys. **73**, 307 (2001).
[16] I. Bloch, J. Dalibard, and W. Zwerger, Rev. Mod. Phys. **80**, 885 (2008).
[17] S. Giorgini, L. P. Pitaevskii, and S. Stringari, Rev. Mod. Phys. **80**, 1215 (2008).
[18] C. Chin, R. Grimm, P. Julienne, and E. Tiesinga, Rev. Mod. Phys. **82**, 1225 (2010).
[19] C. Chin, M. B. A. Altmeyer, S. Riedl, S. Jochim, J. H. Denschlag, and R. Grimm, Science **305**, 1128 (2004).
[20] C. A. Regal, M. Greiner, and D. S. Jin, Phys. Rev. Lett. **92**, 040403 (2004).
[21] M. W. Zwierlein, C. A. Stan, C. H. Schunck, S. M. F. Raupach, A. J. Kerman, and W. Ketterle, Phys. Rev. Lett. **92**, 120403 (2004).
[22] G. B. Partridge, K. E. Strecker, R. I. Kamar, M. W. Jack, and R. G. Hulet, Phys. Rev. Lett. **95**, 020404 (2005).
[23] T.-L. Ho and R. B. Diener, Phys. Rev. Lett. **94**, 090402 (2005).
[24] V. Gurarie and L. Radzihovsky, Ann. Phys. **322**, 2 (2007).
[25] C.-H. Cheng and S.-K. Yip, Phys. Rev. Lett. **95**, 070404 (2005).

[26] J. Zhang, E. G. M. van Kempen, T. Bourdel, L. Khaykovich, J. Cubizolles, F. Chevy, M. Teichmann, L. Tarruell, S. J. J. M. F. Kokkelmans, and C. Salomon, Phys. Rev. A **70**, 030702(R) (2004).
[27] J. P. Gaebler, J. T. Stewart, J. L. Bohn, and D. S. Jin, Phys. Rev. Lett. **98**, 200403 (2007).
[28] J. Fuchs, C. Ticknor, P. Dyke, G. Veeravalli, E. Kuhnle, W. Rowlands, P. Hannaford, and C. J. Vale, Phys. Rev. A **77**, 053616 (2008).
[29] Y. Inada, M. Horikoshi, S. Nakajima, M. Kuwata-Gonokami, M. Ueda, and T. Mukaiyama, Phys. Rev. Lett. **101**, 100401 (2008).
[30] G. Grynberg, B. Lounis, P. Verkerk, J. Y. Courtois, and C. Salomon, Phys. Rev. Lett. **70**, 2249 (1993).
[31] C. Wu, D. Bergman, L. Balents, and S. Das Sarma, Phys. Rev. Lett. **99**, 070401 (2007).
[32] C. Wu and S. Das Sarma, Phys. Rev. B **77**, 235107 (2008).
[33] S. Z. Zhang, H. H. Hung, and C. Wu (to appear in Phys. Rev. A), e-print arXiv:0805.3031.
[34] C. Wu, Phys. Rev. Lett. **100**, 200406 (2008).
[35] C. Wu, Phys. Rev. Lett. **101**, 186807 (2008).
[36] P. G. De Gennes, *Superconductivity of Metals and Alloys* (Addison-Wesley, Reading, MA, 1989).
[37] J. J. McClelland and J. L. Hanssen, Phys. Rev. Lett. **96**, 143005 (2006).
[38] Y. He, Q. Chen, and K. Levin, Phys. Rev. A **72**, 011602 (2005).
[39] A. Schirotzek, Y. I. Shin, C. H. Schunck, and W. Ketterle, Phys. Rev. Lett. **101**, 140403 (2008).
[40] M. Lu, S. H. Youn, and B. L. Lev, Phys. Rev. Lett. **104**, 063001 (2010).
[41] H. H. Hung, W. C. Lee, and C. Wu, e-print arXiv:0910.0507.